Batteries & Supercaps

Research Article
doi.org/10.1002/batt.202500227

Chemistry Europe
European Chemical Societies Publishing

www.batteries-supercaps.org

Stabilizing the Solid Electrolyte Interphase with Phenyl Isothiocyanate for Long-Cycle Lithium Metal Batteries

Bushra Khan, Mohammad Nasir, Jae-won Lee, and Hee Jung Park*

Lithium metal batteries possess great potential for portable electronic devices as a next-generation secondary battery owing to their high specific capacity and energy density. However, their cycling stability is hindered by the formation of an unstable solid-electrolyte interphase between the electrolyte and the Li anode, leading to poor cycling performance. Herein, phenyl isothiocyanate (PITC) has been introduced as an additive in a propylene carbonate (PC) electrolyte to stabilize the solid-electrolyte interphase layer on the Li metal anode. The addition of PITC significantly improves the electrochemical performance of Li||Cu half-cells, exhibiting a coulombic efficiency of 82%, and enhances cycling stability in Li||Li symmetric cells, with low polarization and a uniform solid-electrolyte interface, as confirmed by scanning electron microscopy (SEM) analysis. In Li||LFP full cells, the optimized electrolyte demonstrated excellent cycling stability, maintaining a discharge capacity of 150 mAh g^{-1} after 650 cycles at a 1C rate. These results verify that PITC is an effective additive for PC-based electrolytes, enhancing the longevity and stability of lithium metal batteries.

1. Introduction

Batteries are one of the most versatile and scalable energy storage technologies, playing a crucial role in facilitating the transition to renewable energy sources.[1,2] While lithium-ion batteries (LIBs) are the current standard for energy storage in portable electronics and electric vehicles, their energy density is approaching its theoretical limit. To meet future energy demands, lithium metal batteries (LMBs) have emerged as a promising alternative due to their significantly higher theoretical capacity (3860 mAh g^{-1} for Li metal compared to 372 mAh g^{-1} for graphite) and energy density.[3,4] However, their commercialization is hindered by several challenges: 1) a fragile and unstable solid-electrolyte interphase (SEI) layer on the Li metal anode, leading to significant volumetric and morphological changes during cycling, 2) limited cycling stability and poor coulombic efficiency (CE), which can cause safety issues such as fire risks, and 3) the uncontrolled growth of Li dendrites during Li plating and stripping, which further degrades battery performance.[5,6]

Numerous strategies have been proposed to address the aforementioned challenges, including the use of high-modulus solid electrolytes to physically inhibit dendrite growth,[7–9] the modification of separators to regulate ion flow,[10] and the development of advanced current collectors to reduce local current density.[11–14] Additionally, approaches such as introducing artificial SEI layers[15,16] and optimizing electrolytes[17–21] have been explored. Among these, electrolyte optimization offers a uniquely integrated and cost-effective solution by facilitating the in situ formation of a stable and compact SEI layer that minimizes dendrite growth and extends battery life.[22]

Several additives, such as fluoroethylene carbonate,[23] lithium difluorophosphate,[24] $LiNO_3$, and vinylene carbonate,[25] have been demonstrated to enhance the performance and stabilize the SEI layer.[26–28] However, they often fail to effectively suppress dendrite growth or maintain a stable passivation layer in carbonate-based electrolytes for LMBs.[29] Literature reports that $LiNO_3$, effective in ether electrolytes, has poor solubility in carbonate systems, limiting SEI stability.[30] Similarly, fluoroethylene carbonate forms a LiF-rich SEI but often results in high resistance, with Li||NMC cells retaining only 65% capacity after 100 cycles.[31]

Isocyanate and isothiocyanate additives have recently garnered significant attention due to their ability to form N-, S-, and F-rich SEI layers. For instance, Han et al. reported trimethylsilyl isothiocyanate as an additive that scavenges hydrofluoric acid (which degrades electrodes and reduces cycling stability) and facilitates the formation of an inorganic-rich SEI layer on both the anode and cathode.[32] Similarly, Guo et al. introduced a novel additive, ethyl isothiocyanate (EITC), to address the cointercalation issues of propylene carbonate (PC) in graphite. Due to its self-polymerization property, EITC polymerizes on the graphite surface, forming a protective layer that prevents solvent intercalation into graphene layers. This resulted in prolonged cycling of Gr||$Li_4Ti_5O_{12}$ cells, achieving a discharge capacity of 140 mAh g^{-1} for up to 500 cycles.[33] Zhang et al. also utilized EITC as an electrolyte additive to stabilize the Li anode in a carbonate electrolyte containing $LiPF_6$ salt. EITC reduced the production of ethylene carbonate (EC) and increased the generation of LiF, forming an SEI layer enriched with LiF and

B. Khan, M. Nasir, H. J. Park
Department of Materials Science and Engineering
Dankook University
Dandae-ro 119, Cheonan 31116, Korea
E-mail: parkjang@dankook.ac.kr

M. Nasir, H. J. Park
Hydrogen Research Center
Dankook University
Dandae-ro 119, Cheonan 31116, Korea

J. Lee
Department of Energy Engineering
Dankook University
Dandae-ro 119, Cheonan 31116, Korea

Supporting information for this article is available on the WWW under https://doi.org/10.1002/batt.202500227

Research Article
doi.org/10.1002/batt.202500227
Chemistry Europe
European Chemical Societies Publishing

cross-linked EITC polymers. This led to stable cycling of Li||LFP cells at a 0.2C rate for 200 cycles.[34] Additionally, 4-fluorophenyl isocyanate formed a robust, N-rich cathode electrolyte interface, thereby improving lithium-ion transport.[35] From these findings, it can be concluded that isothiocyanate groups and benzene rings hold significant potential as effective additives for improving SEI stability and suppressing dendrite growth in LMBs. In this study, phenyl isothiocyanate (PITC) is introduced as a novel additive for carbonate-based electrolytes in LMBs. PITC is composed of an aromatic ring and an isothiocyanate group, which impart multifunctional properties. The isothiocyanate group promotes the formation of an SEI layer enriched with LiF, Li_3N, and sulfates and facilitates self-polymerization, while the benzene ring facilitates π–π stacking, improving Li-ion transport and the mechanical strength of the SEI layer.[36] These properties effectively inhibit Li dendrite formation, minimize side reactions, and improve long-term cycling stability. Consequently, Li||$LiFePO_4$ (LFP) cells incorporating 2 wt% of PITC demonstrated excellent cycling stability, achieving up to 650 cycles with 98% capacity retention at a 1C rate. To the best of our knowledge, this study is the first to investigate PITC as an electrolyte additive for LMBs, offering a novel strategy to address the challenges associated with carbonate-based electrolytes.

2. Result and Discussion

2.1. Selection Criteria for Additives

Various additives have been investigated in the literature to form a stable SEI layer in LMBs. Quantum mechanical calculations were adopted to estimate the energy levels of the electrolyte components PC, lithium salt LiTFSI, and PITC, as shown in **Figure 1**a,

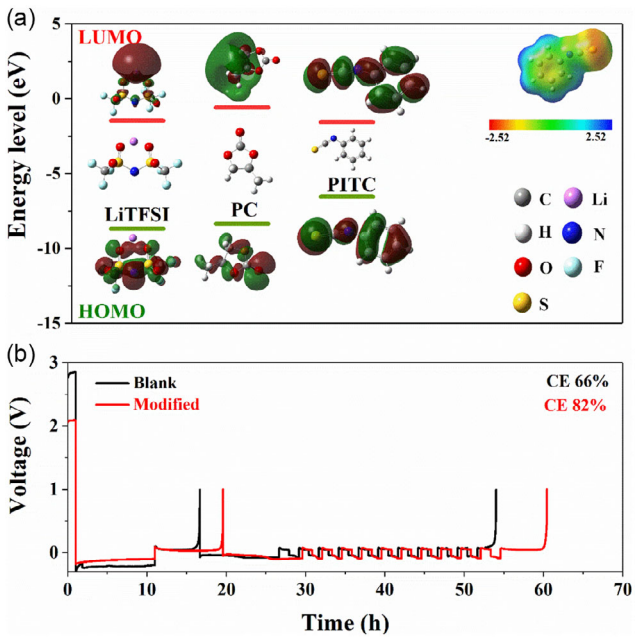

Figure 1. a) HOMO and LUMO energies level of all the components of the electrolyte (LiTFSI, PC, PITC) and b) columbic efficiencies of Li||Cu cell with blank and modified electrolyte.

using Gaussian 16 at the B3LYP/6-311++G (d, p) level of theory.[37,38] PITC shows a lower LUMO (lowest unoccupied molecular orbital) and a higher HOMO (highest occupied molecular orbital) compared to the salt and solvent. PITC has two functional groups: a phenyl ring and an isothiocyanate (–N═C═S) group.[39] Due to π–π interactions, the phenyl group stacks over one another, facilitating molecular arrangement and improving Li-ion conductivity.[36] Meanwhile, the isothiocyanate group can undergo self-polymerization on the anode surface. PITC is expected to oxidize and reduce preferentially before other electrolyte components, forming a passivation layer on the surfaces of both the anode and cathode. This layer efficiently prevents side reactions and generates an SEI layer enriched with inorganic components such as LiF, Li_3N, and sulfates.

2.2. Electrochemical properties of Li||Cu Cells

Carbonate solvents such as EC and PC are widely used in LIBs. However, their use in LMBs has been limited due to their tendency to form an unstable SEI layer, which leads to Li dendrite formation on the Li metal anode.[40] To overcome this issue, a novel additive, PITC, was added to PC, and its effect on the electrochemical properties of LMBs was systematically investigated. Figure 1b shows the galvanostatic cycling profiles of Li||Cu cells containing blank and modified electrolytes at a current density of 0.4 mA cm^{-2} and a capacity of 0.5 mAh cm^{-2} . The first 10 cycles were recorded, followed by continuous stripping up to a cutoff voltage of 1 V, as per the procedure reported by Adams et al.[41] The CE increased from 66% in the blank electrolyte to 82% in the modified electrolyte. This indicates that PITC effectively influenced the plating and stripping behavior of Li metal by facilitating the formation of a stable SEI layer enriched with beneficial inorganic components. To further explore the kinetic behavior of Li ions, Li||Cu cells were examined at higher current densities of 0.1C and 1C (Figure S1, Supporting Information). The blank electrolyte exhibited high voltage polarization and nucleation overpotential, while the modified electrolyte displayed significantly lower voltage polarization and nucleation overpotential, highlighting improved Li-ion transport and more uniform Li deposition.

The morphology of deposited Li was further investigated to understand the influence of PITC on Li plating behavior. Li||Cu cells were cycled at current densities of 0.25 and 1.0 mA cm^{-2} for 6 and 24 h, respectively. Subsequently, the cells were disassembled, and the Cu substrate was analyzed, as shown in **Figure 2**. Nonuniform Li deposition was evident from the digital images of the Cu foil in the blank electrolyte, with significant portions of the Cu substrate remaining uncovered (Figure 2a,b). This uneven Li deposition is attributed to poor Li dynamics and high nucleation in the blank electrolyte. On the other hand, the addition of PITC resulted in smooth, dense, and homogeneous Li deposition, fully covering the Cu substrate with a uniform silver-white appearance (Figure 2c,d). This implies that the PITC additive improves Li plating behavior by enhancing Li^+ transport and enabling controlled nucleation. To directly assess Li^+ kinetics, ionic conductivity measurements were

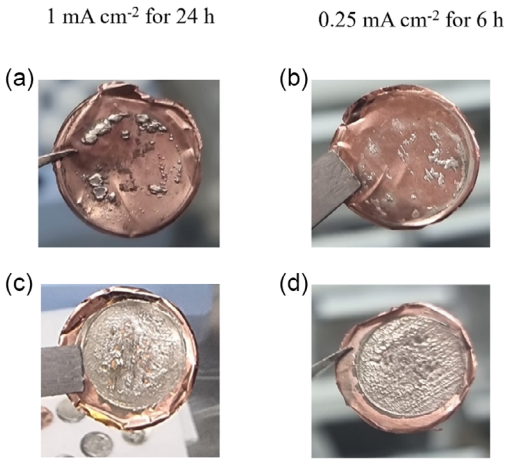

Figure 2. Digital images of Li deposition on Cu substrate cycled with a,b) blank and c,d) modified electrolyte.

performed using the electrochemical impedance spectroscopy (EIS) method with sus||sus cells and a polyethylene terephthalate film as the separator (Figure S2 and Table S2, Supporting Information). The obtained conductivity value was 1.88 mS cm^{-1} for the blank electrolyte, which increased to 2.39 mS cm^{-1} for the modified electrolyte.

2.3. Electrochemical Properties of Li||Li Symmetric Cell

Li||Li symmetric cells with the blank and modified electrolytes were assembled to validate the impact of PITC on SEI layer formation and cycling behavior. The cells were tested at a current density of 0.5 mA cm^{-2}, with plating and stripping times of 1 h. **Figure 3**a shows the voltage profiles for the blank and modified electrolytes during long-term cycling at 25 °C. The overpotential of the cell with the blank electrolyte began to rise after 275 h, and the cell ultimately failed after 325 h. This behavior can be attributed to the unstable SEI layer and dendritic growth, leading to higher polarization (≈362 mV). On the other hand, the cell with the modified electrolyte cycled well for up to ≈375 h, exhibiting lower nucleation overpotential and voltage polarization (≈151 mV). These results indicate that the addition of PITC facilitates the formation of a durable and ion-conductive SEI layer on the Li metal anode, which mitigates Li dendrite growth and improves the stability of Li plating and stripping.

EIS was further conducted to evaluate the robustness and compatibility of the SEI layer and its impact on interfacial resistance. Impedance measurements were carried out for the Li||Li symmetric cells operated at 0.5 mA cm^{-2} for the blank and modified electrolytes before and after the 25th, 50th, 100th, and 150th cycles. Nyquist plots of EIS for the blank and modified electrolytes are shown in Figure 3b,c, respectively. The initial point of intersection with the x-axis in the high-frequency region was attributed to the resistance of the electrolytes, or Ohmic resistance (R_e). The first semicircle, from the high to medium-frequency region, was associated with SEI layer resistance (R_{SEI}), whereas the second semicircle in the medium-frequency region corresponded to the charge transfer resistance (R_{ct}).[24,42] Figure 3b demonstrates that the resistance tends to increase with cycling, and there is a significant increase in resistance after 150 cycles due to short circuit. However, in Figure 3c, less resistance increased with cycling after 150 cycles. The impedance data were analyzed using a modified Randles–Ershler equivalent circuit, shown as an inset in Figure 3d (where CPE_{SEI} denotes the constant phase element linked with R_{SEI} and CPE_{ct} corresponds to the constant phase element associated with R_{ct}).[43,44] Initially, both electrolyte systems revealed high total resistance $R_T = (R_{SEI} + R_{ct})$ before cycling due to the absence of a stable SEI layer. Significant differences in the total resistance of the blank and additive-modified electrolytes were observed during cycling. As shown in Figure 3d, the total resistance $R_T = (R_{ct} + R_{SEI})$ of the blank electrolyte remained unstable due to the continuous renewal and rupture of the passivation layer during repeated deposition and stripping of Li metal. This instability led to a dramatic increase in resistance by the 150th cycle, resulting in high polarization and poor cycling performance of the cell (Figure 3a). However, the Li||Li cell with the modified electrolyte demonstrated stable and lower resistance throughout the cycling process. In addition, R_{SEI} and R_{ct} were observed to consistently lower for modified system, emphasizing the formation of a robust and uniform SEI layer. Thus, it is established that PITC-induced SEI layer suppressed the dendritic lithium growth and reduced interfacial resistance, promoting improved electrochemical kinetics.[45] The exceptionally stable SEI layer played a significant role in maintaining the performance and longevity of the battery.

To evaluate the morphology of the SEI layer, Li||Li symmetric cells were cycled at a current density of 0.5 mA cm^{-2} for 65, 100, and 150 cycles. After cycling, the cells were disassembled, and the Li foils were analyzed using scanning electron microscopy (SEM) to observe morphological changes in SEI layer formation in the blank and modified electrolyte systems. **Figure 4**a–c shows the top surface SEM images of the Li anodes cycled in the blank electrolyte. The Li surfaces appear highly irregular, displaying a fractured, porous, and moss-like structure. With the increase in cycling, the surface gets more uneven and rough, which indicates the growth of Li dendrites. These unstable morphologies reveal the formation of a thick and unstable SEI layer that could not effectively protect the surface of the Li anode. The development of such a layer restricts Li-ion transport through the interface, resulting in a large overpotential during cycling, as shown in Figure 3.[46] Corresponding cross-sectional images along the cycling further confirm the degree of SEI layer deterioration and decomposition of electrolyte, revealing that the thickness of eroded layer on the Li surface continuously increases with cycling from 55 to 223 μm, as illustrated in Figure 4g–i. The thick, loosely attached SEI layer indicates the continuous formation and rupturing of the SEI layer, which leads to poor performance and cell failure. Interestingly, the Li anode cycled in the modified electrolyte exhibits significantly improved morphology. Figure 4d–f displays top-view SEM images for the modified electrolyte. The Li surface appears smooth, dense, and uniformly deposited, with minimal irregularities. Additionally, compact and spherical structures indicate a more controlled and uniform Li deposition process. Cross-sectional analysis reveals a compact, clean, and much thinner SEI layer as compared to blank electrolyte (24 to 77.3 μm)

Research Article
doi.org/10.1002/batt.202500227
Chemistry Europe
European Chemical Societies Publishing

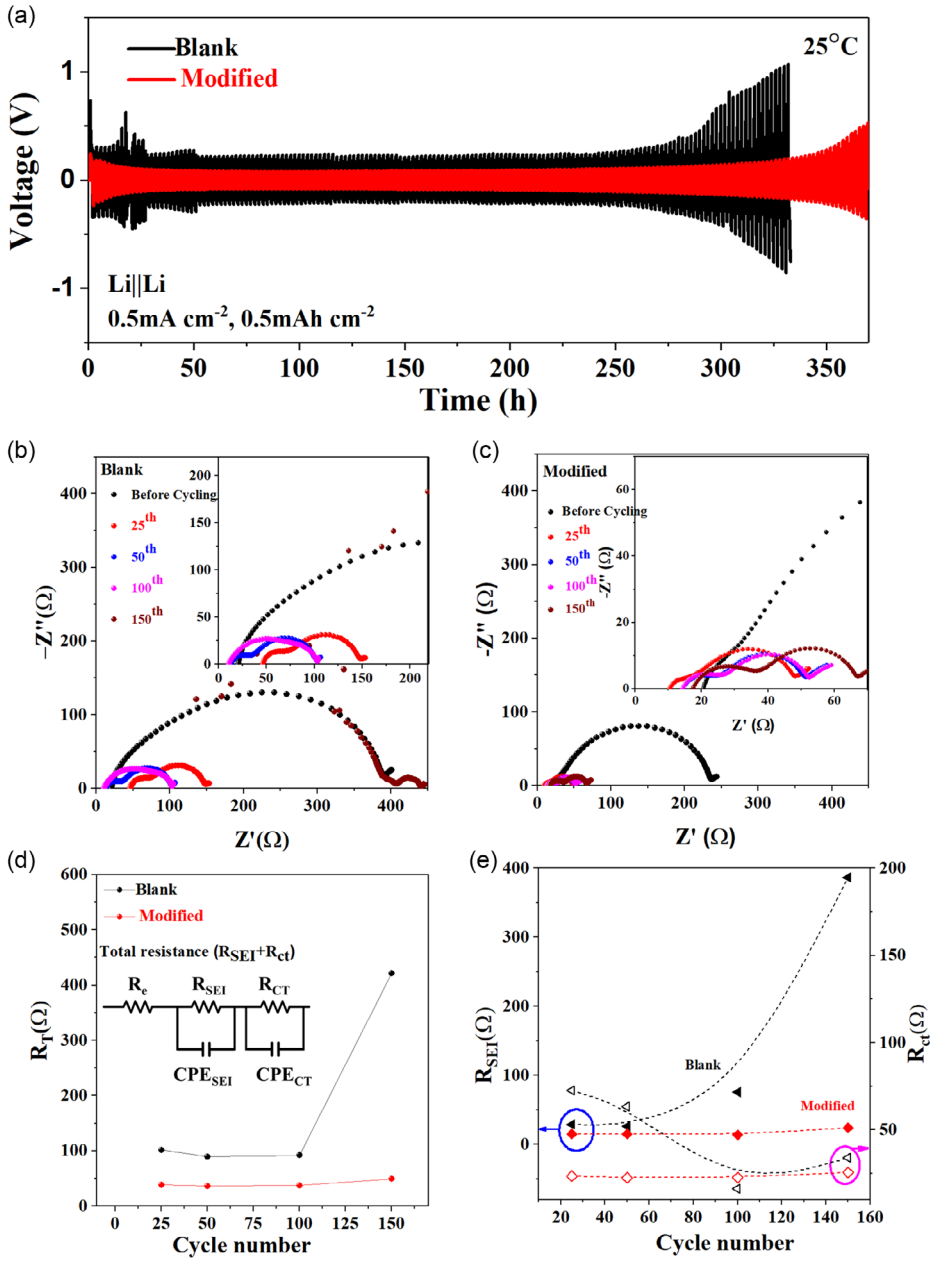

Figure 3. a) Cycling performance of Li||Li symmetric cells with blank and modified electrolyte. EIS of Li||Li symmetric cells before and after cycling for b) blank and c) modified electrolytes. d) Total resistance $R_T = (R_{ct} + R_{SEI})$ and e) resistances of SEI layer and charge transfer of blank and modified electrolytes.

that is strongly adhered to the Li surface, as shown in Figure 4j–l.[47] This uniform SEI layer acts as an effective passivation layer, facilitating homogeneous Li-ion transport and minimizing overpotential during cycling. These morphological findings explain the improved electrochemical performance of the modified electrolyte in Li||Li symmetric cells.

To investigate the chemical composition and structure of the SEI layer formed on the lithium metal surface, X-ray photoelectron spectroscopy (XPS) analysis was conducted on Li anodes retrieved from Li||Li symmetric cells after 65 cycles using both blank and PITC-modified electrolytes. The deconvoluted spectra for C 1*s*, O 1*s*, N 1*s*, Li 1*s*, and S 2*p* are shown in **Figure 5**. In the C 1*s* spectra, the blank sample exhibits a dominant peak at 285.0 eV corresponding to C—C/C—H bonds, along with minor peaks at ≈289.0 and ≈286.5 eV attributed to C═O and C—O bonds, respectively (Figure 5a(i)). These signals indicate a high concentration of unstable organic species in the SEI, which are prone to dissolution in carbonate electrolytes, resulting in repeated SEI rupture and regeneration. In contrast, the modified sample displays additional peaks at 286.6 eV (C═N) and 283.2 eV (C—S—C) (Figure 5a(ii)), confirming the decomposition of PITC and the formation of a PITC-derived polymer film. This polymer-rich SEI helps suppress further electrolyte decomposition and contributes to improved passivation. The O 1*s* spectra further support these observations. The blank electrolyte shows a strong peak at 532.7 eV due to Li_2CO_3 and smaller peaks assigned to LiOH

Research Article
doi.org/10.1002/batt.202500227
Chemistry Europe
European Chemical Societies Publishing

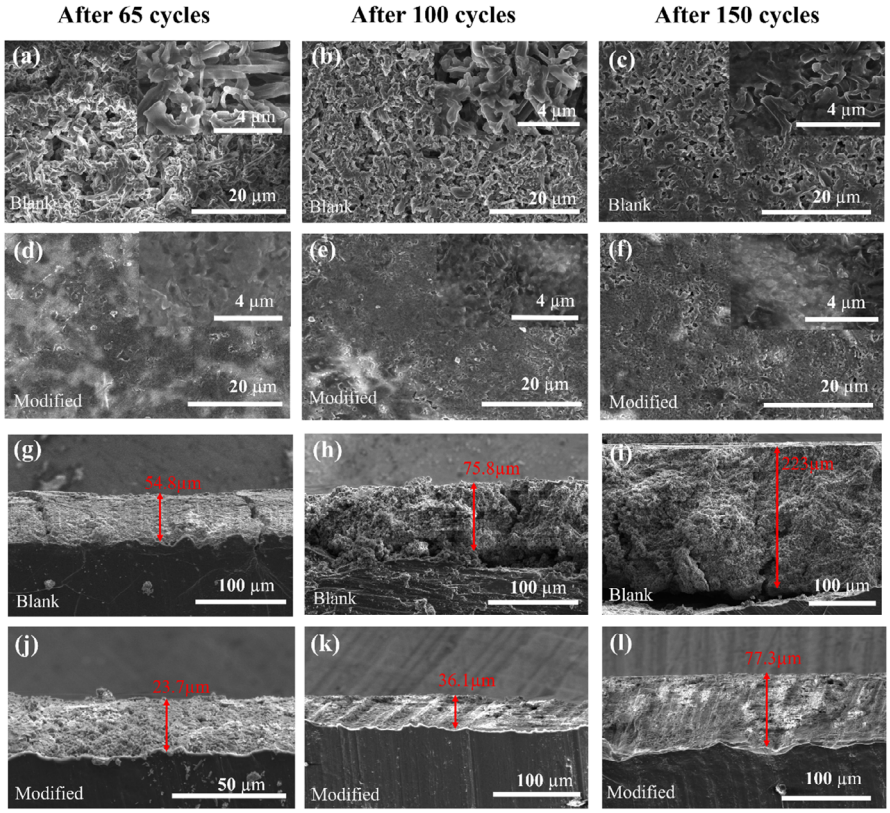

Figure 4. SEM images after cycling Li||Li symmetric cells for 65, 100, and 150 cycles a–c) top and g–i) cross-sectional images for blank electrolyte. d–f) top and j–l) cross-sectional images for the modified electrolyte.

and $ROCO_2Li$ (Figure 5b(i)), indicative of severe electrolyte decomposition. In the modified electrolyte, the Li_2CO_3 peak is reduced (Figure 5b(ii)), suggesting suppressed carbonate formation due to the protective PITC layer.

In the N 1*s* spectra, the blank sample only shows a peak associated with residual LiTFSI, suggesting minimal nitrogen-based SEI contribution (Figure 5c(i)). However, in the modified sample, an additional peak emerges at 398.4 eV (C—N) (Figure 5c(ii)), consistent with the presence of polymerized PITC species, along with a shoulder assigned to Li_3N, indicating the participation of PITC decomposition products in SEI formation. The Li 1*s* spectra also reflect distinct differences. In the blank electrolyte, the SEI comprises Li_2CO_3 and a relatively small amount of LiF ($LiF/Li_2CO_3 = 0.89$) (Figure 5d(i)). In the modified sample, the intensity of LiF increases and a new Li_3N peak appears (Figure 5d(ii)), with LiF/Li_2CO_3 and Li_3N/Li_2CO_3 ratios of 1.59 and 1.23, respectively. The S 2*p* spectra show that the blank sample contains a dominant LiTFSI signal and a small SO_4^{2-} peak, with a SO_4^{2-}/LiTFSI ratio of 0.89 (Figure 5e(i)), indicating limited sulfur-based SEI formation. In the modified electrolyte, the S 2*p* spectrum shows a decreased SO_4^{2-}/LiTFSI ratio of 0.45 and the emergence of $S_2O_3^{2-}$ with a S_2O_3/LiTFSI ratio of 0.12 (Figure 5e(ii)), attributed to PITC decomposition.

LiF contributes to chemical stability and suppresses dendritic growth by forming a compact and inert interface.[48] Li_3N, with its high ionic conductivity ($\approx 10^{-3}$ S cm^{-1}), facilitates efficient Li^+ transport across the SEI.[49] Their coexistence creates a synergistic effect, enhancing both stability and charge transfer.[28,50] Additionally, $S_2O_3^{2-}$ improves the elasticity of the SEI, allowing it to accommodate volume changes and resist cracking during cycling, as reported in recent studies.[51,52] Thus, SEI formed in the modified electrolyte rich in LiF, Li_3N, and thiosulfates offers improved chemical stability, enhanced Li^+ transport, and greater mechanical integrity compared to the SEI formed with the blank electrolyte.

2.4. Electrochemical Performance of Li||LFP Full Cell

The olivine-structured LFP cathode material has garnered significant research interest due to its affordability, nontoxicity, safety, and thermal stability, making it a promising choice for LMBs.[53,54] Therefore, Li||LFP cells featuring Li as the anode and LFP as the cathode were investigated using galvanostatic cycling to compare the performance of the blank and modified electrolytes. Two formation cycles were conducted at a 0.1C rate to ensure the development of a robust protective layer on both the anode and cathode. During these cycles, the blank and modified electrolytes delivered discharge capacities of 170 and 138 mAh g^{-1} (at 0.1C rate), respectively, with almost identical coulombic efficiencies (98%). Subsequent cycling was performed at a 1C rate to assess performance, and the results for the modified electrolyte are displayed in Figure S3, Supporting Information. The discharge capacity and CE for the blank and modified electrolytes are shown in **Figure 6**a. The Li||LFP cell with the blank electrolyte

Research Article
doi.org/10.1002/batt.202500227
Chemistry Europe
European Chemical Societies Publishing

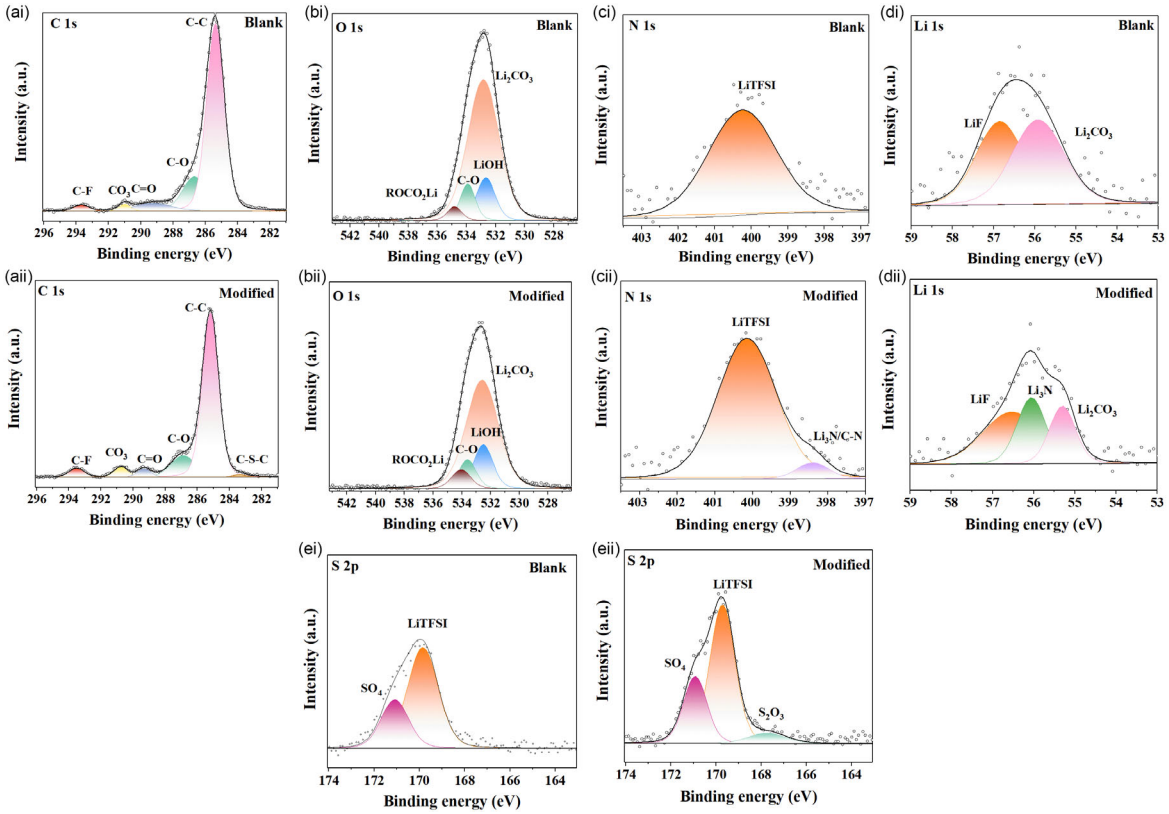

Figure 5. XPS spectra of Li anode after cycling Li||Li symmetric cells for 65 cycles at different edges: a) C 1s, b) O 1s, c) Li 1s, d) N 1s, and e) S 2p for i) blank and ii) modified electrolytes.

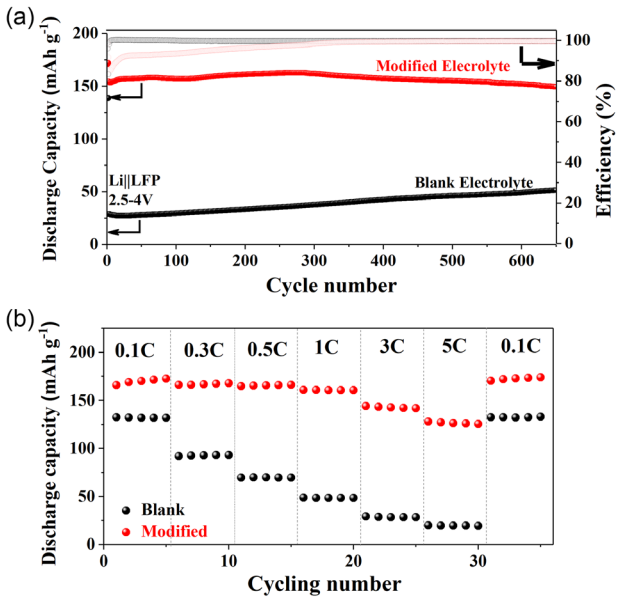

Figure 6. a) Discharge capacity and CE and b) rate performance test of Li|| LFP cells fabricated with blank and modified electrolytes.

exhibited a rapid decline in discharge capacity, achieving only ≈50 mAh g^{-1} after 650 cycles. This poor performance is attributed to the instability of the electrolyte with the Li anode and parasitic reactions of the electrolyte on both electrodes, as observed earlier. However, the cell with the modified electrolyte demonstrated stable cycling performance, attaining a discharge capacity of ≈150 mAh g^{-1} with excellent capacity retention of 98% over 650 cycles. These results clearly highlight the importance of the PITC additive in stabilizing the electrolyte with both electrodes. Table S3, Supporting Information, provides a comparison of the cycling performance of the modified electrolyte with traditional electrolyte systems containing various additives. From the table, it is evident that the modified electrolyte with 2 wt% PITC exhibits relatively better discharge capacity and cycling stability compared to previously reported conventional electrolytes. To gain deeper insight into the electrode/electrolyte interface, dQ/dV curves were analyzed for the initial cycle (Figure S4, Supporting Information). The blank electrolyte shows two broad, low-amplitude peaks, indicating its instability with the LFP cathode. However, the modified electrolyte reveals a sharp, high-amplitude peak in the dQ/dV curve, emphasizing the formation of uniform CEI and SEI layers enriched with inorganic species.[55,56]

The applied current density significantly influences the electrochemical properties of the Li anode, particularly Li deposition and growth.[57,58] To examine this effect, Li||LFP cells were tested with blank and modified electrolytes at various current densities. At the lowest current density (0.1C), both electrolytes showed comparable discharge capacities. However, as the current density increased, a notable difference in performance was observed (Figure 6b and Figure S5, Supporting Information). The battery with the

modified electrolyte delivered superior rate capabilities, achieving discharge capacities of 165, 165, 164, 160, 144, and 130 mAh g^{-1} at 0.1C, 0.3C, 0.5C, 1C, 3C, and 5C rates, respectively. On the other hand, the blank electrolyte exhibited drastic capacity fading at higher current densities, delivering only 19 mAh g^{-1} at 5C, compared to 130 mAh g^{-1} for the modified electrolyte. After completing the performance tests (30 cycles), the cells were retested at 0.1C to evaluate capacity recovery. The modified electrolyte demonstrated complete recovery, achieving the original discharge capacity of ≈165 mAh g^{-1}, suggesting minimal parasitic reactions even at higher currents (5C).[59] However, cells containing the blank electrolyte demonstrated a significant decrease in discharge capacities (≈138 mAh g^{-1}), indicating increased side reactions and instability at the electrolyte/electrode interface. Thus, the superior performance of the modified electrolyte is directly linked to the role of the PITC additive in stabilizing the SEI/CEI layers with negligible interfacial resistance, as evidenced by the EIS results for Li||Li symmetric cells (refer to Figure 3). When subjected to electrochemical reduction, PITC undergoes reductive decomposition due to its lower LUMO energy level compared to the PC solvent and LiTFSI salt. This decomposed PITC primarily interacts with Li ions, resulting in the formation of essential inorganic compounds such as LiF, Li_3N, and sulfates. These byproducts play a vital role in enhancing the stability and functionality of the SEI layer.[33] The isothiocyanate functional group (–N═C═S) in PITC is highly reactive, with the sulfur (S) and nitrogen (N) atoms contributing to the generation of Li_2SO_4, S_2O_3, and Li_3N compounds, respectively. These products form a mechanically robust and ionically conductive SEI layer that inhibits Li dendrite formation and reduces electrolyte decomposition. Furthermore, the phenyl group acts as a structural anchor, promoting uniform SEI formation across the Li surface. The preferential decomposition of PITC over PC ensures effective passivation of the Li surface, significantly reducing ongoing side reactions and facilitating stable long-term cycling in LMBs.

3. Conclusions

The role of PITC as an effective additive for single-solvent carbonate electrolytes to enhance the performance of LMBs is thoroughly investigated. PITC induces the formation of a strong and compact SEI layer, rich in LiF, Li_3N, Li_2SO_4, and S_2O_3, which stabilizes the Li metal anode by suppressing dendrite growth and side reactions. Consequently, symmetric Li||Li cells incorporating PITC demonstrate low polarization and improved cycling stability compared to those without the additive. Similarly, Li||Cu cells exhibit enhanced CE, confirming their role in stabilizing lithium plating and stripping. As expected, for Li||LFP cells, the modified electrolyte system delivered a high discharge capacity (≈150 mAh g^{-1}) with 98% retention over 650 cycles, along with excellent rate performance and capacity recovery at high current densities. Thus, PITC as an additive possesses considerable potential for application in rechargeable batteries to improve cycling performance.

4. Experimental Section

The commercial products PC (battery grade 98%, TCI Chemicals), PITC (>98%, TCI Chemicals), and bis(trifluoromethyl sulfonyl)amine lithium salt (LiTFSI, 99.95% trace metals basis, Sigma-Aldrich) were used for the preparation of electrolytes. A 1M LiTFSI salt was dissolved in PC to obtain the reference carbonate-based electrolyte, labeled as the blank electrolyte. To prepare the modified electrolyte, 2 wt% of PITC was mixed into the blank electrolyte.

For cell fabrication, Li metal foil (MTI Corporation) with a diameter of 14 mm and a thickness of 250 μm was used as the anode. The cathode was prepared by creating a slurry consisting of 80 wt% $LiFePO_4$ (MTI Corporation) active material, 5 wt% Super-P (Imerys Graphite & Carbon), and 10 wt% polyvinylidene fluoride (PVDF, MW 44 080, Alfa Aesar) dissolved in N-methyl-2-pyrrolidone (NMP, Samchun 99.5%). The uniformly mixed slurry was spread onto aluminum foil (MTI Corporation) using the doctor blade technique. Subsequently, the electrodes were dried at 80 °C for 12 h and cut into 10 mm diameter disks. The LFP cathodes were further dried at 80 °C under vacuum for 12 h before use. Polypropylene (PP) separator Celgard 2400 and copper (Cu) foil were purchased from the Wellcos Corporation.

The morphological changes and composition of the surface components of the SEI layer developed on the surface of the Li anode were analyzed using field-emission scanning electron microscopy (MSE40 UHR FE-SEM) and XPS (Scientific K-Alpha system, Thermo Scientific). The electrochemical performance of the electrolytes was evaluated using 2032-coin cells. Cells were assembled in an argon-filled glove box (<0.1 ppm oxygen and <0.1 ppm H_2O) using 60 μL of electrolyte, with polypropylene separators (PP) and electrodes predried under vacuum. All galvanostatic cycling experiments were executed with a WBCS3000L battery cycler (purchased from Wonatech, Korea).

Li||Cu cells were tested to assess their CE using Method 3 described by Adam et al., where Cu foil acted as the substrate during Li metal plating and stripping. Li||Li symmetric cells were cycled at a current density of 0.5 mA cm^{-2} for 65, 100, and 150 cycles at 25 °C. Thereafter, the Li anode was investigated to observe SEI layer formation. Li||Li symmetric cells were further cycled galvanostatically at 0.5 mA cm^{-2} with a capacity of 0.5 mAh cm^{-2} per cycle to evaluate the polarization and cycling stability of the electrolytes. For Li||LFP cells, galvanostatic charge/discharge tests were conducted within a voltage range of 2.5 to 4.0 V. The cells were first activated for two formation cycles at a 0.1C rate to ensure electrode stabilization. Subsequently, cycling tests were conducted at 1C (1C = 160 mAh g^{-1} for Li||LFP) for both the charge and discharge steps. For C-rate tests, the Li||LFP cells were cycled at increasing rates of 0.2C , 0.5C , 1.0C , 2.0C , and 3.0C, then returned to 0.1C to explore the rate capability and capacity recovery. EIS was performed using a Zurich Instruments MFIA Impedance Analyzer over a frequency range of 1 Hz to 5 MHz with an AC voltage amplitude of 10 mV. The ionic conductivity of the electrolytes was determined by fabricating sus||sus cells using the EIS method.

Acknowledgements

This work was supported by the National Research Foundation of Korea (NRF) grant funded by the Korea government (MSIT) (no. RS-2023-00236572).

Conflict of Interest

The authors declare no conflict of interest.

Author Contributions

Bushra Khan: data curation (lead); investigation (lead); writing—original draft (equal). **Mohammad Nasir**: data curation (equal); investigation (supporting); writing—original draft (supporting). **Jae-won Lee**: data curation (supporting); investigation (supporting). **Hee Jung Park**: conceptualization (equal); funding acquisition (lead); investigation (lead); supervision (lead); writing—original draft (supporting); writing—review and editing (lead).

Data Availability Statement

The data that support the findings of this study are available from the corresponding author upon reasonable request.

Keywords: carbonate electrolytes · Li anodes · lithium metal batteries · phenyl isothiocyanate · solid-electrolyte interphase

[1] M. A. Rajaeifar, P. Ghadimi, M. Raugei, Y. Wu, O. Heidrich, *Resour. Conserv. Recycl.* **2022**, *180*, 106144.
[2] Ş. Kılkış, G. Krajačić, N. Duić, M. A. Rosen, M. Ahmad Al-Nimr, *Energy Convers. Manag.* **2021**, *245*, 114606.
[3] T. A. Faunce, J. Prest, D. Su, S. J. Hearne, F. Iacopi, *MRS Energy Sustain.* **2018**, *5*, 10.
[4] S. Kim, J.-S. Kim, L. Miara, Y. Wang, S.-K. Jung, S. Y. Park, Z. Song, H. Kim, M. Badding, J. Chang, V. Roev, G. Yoon, R. Kim, J.-H. Kim, K. Yoon, D. Im, K. Kang, *Nat. Commun.* **2022**, *13*, 1883.
[5] Q. Wang, B. Liu, Y. Shen, J. Wu, Z. Zhao, C. Zhong, W. Hu, *Adv. Sci.* **2021**, *8*, 2101111.
[6] S. Chen, F. Dai, M. Cai, *ACS Energy Lett.* **2020**, *5*, 3140.
[7] J. Liu, J. Zhou, M. Wang, C. Niu, T. Qian, C. Yan, *J. Mater. Chem. A* **2019**, *7*, 24477.
[8] S. I. Jung, M. Nasir, H. J. Park, *J. Mater. Chem. A* **2025**, *13*, 4624.
[9] L. Braks, J. Zhang, A. Forster, P. Fritz, J. Oh, M. El Kazzi, J. W. Choi, A. Coskun, *Angew. Chem. Int. Ed.* **2024**, *63*, e202408238.
[10] M. F. Lagadec, R. Zahn, V. Wood, *Nat. Energy* **2019**, *4*, 16.
[11] J. S. Park, M. Nasir, D. Kim, H. M. Jeong, H. J. Park, *Batter. Supercaps* **2025**, e202400741, https://doi.org/10.1002/batt.202400741.
[12] B. Zhou, A. Bonakdarpour, I. Stoševski, B. Fang, D. P. Wilkinson, *Prog. Mater. Sci.* **2022**, *130*, 100996.
[13] X.-Y. Yue, X.-L. Li, J. Bao, Q.-Q. Qiu, T. Liu, D. Chen, S.-S. Yuan, X.-J. Wu, J. Lu, Y.-N. Zhou, *Adv. Energy Mater.* **2019**, *9*, 1901491.
[14] H. Jo, J.-W. Lee, E. Kwon, S. Yu, B. G. Kim, S. Park, J. Moon, M. J. Ko, H.-D. Lim, *ACS Nano* **2024**, *18*, 35718.
[15] N.-W. Li, Y.-X. Yin, C.-P. Yang, Y.-G. Guo, *Adv. Mater.* **2016**, *28*, 1853.
[16] J. Wang, J. Yang, Q. Xiao, J. Zhang, T. Li, L. Jia, Z. Wang, S. Cheng, L. Li, M. Liu, H. Liu, H. Lin, Y. Zhang, *Adv. Funct. Mater.* **2021**, *31*, 2007434.
[17] H. Dai, K. Xi, X. Liu, C. Lai, S. Zhang, *J. Am. Chem. Soc.* **2018**, *140*, 17515.
[18] P. Zhou, Y. Xia, W. Hou, S. Yan, H.-Y. Zhou, W. Zhang, Y. Lu, P. Wang, K. Liu, *Nano Lett.* **2022**, *22*, 5936.
[19] M. Nasir, J. Seo, J. S. Park, S. I. Jung, H. J. Kim, H. J. Park, *Ceramist* **2024**, *27*, 1.
[20] J. Seo, M. Nasir, H. J. Park, *ACS Appl. Energy Mater.* **2025**, *8*, 1518.
[21] Z. D. Jin, J. H. Pi, O. Park, K. H. Lee, S. Kim, H. J. Park, *J. Korean Ceram. Soc.* **2024**, *61*, 492.
[22] J. Xie, S.-Y. Sun, X. Chen, L.-P. Hou, B.-Q. Li, H.-J. Peng, J.-Q. Huang, X.-Q. Zhang, Q. Zhang, *Angew. Chem.* **2022**, *134*, e202204776.
[23] T. Hou, G. Yang, N. N. Rajput, J. Self, S.-W. Park, J. Nanda, K. A. Persson, *Nano Energy* **2019**, *64*, 103881.
[24] P. Shi, L. Zhang, H. Xiang, X. Liang, Y. Sun, W. Xu, *ACS Appl. Mater. Interfaces* **2018**, *10*, 22201.
[25] D. Aurbach, K. Gamolsky, B. Markovsky, Y. Gofer, M. Schmidt, U. Heider, *Electrochimica Acta* **2002**, *47*, 1423.
[26] E. P. Kamphaus, S. Angarita-Gomez, X. Qin, M. Shao, M. Engelhard, K. T. Mueller, V. Murugesan, P. B. Balbuena, *ACS Appl. Mater. Interfaces* **2019**, *11*, 31467.
[27] R. Jiang, Z. Zhu, X. Qi, F. Yang, H. Du, J. Ji, R. Zhang, Z. Liu, L. Qie, *Small* **2025**, *21*, 2410486.
[28] Q.-K. Zhang, S.-Y. Sun, M.-Y. Zhou, L.-P. Hou, J.-L. Liang, S.-J. Yang, B.-Q. Li, X.-Q. Zhang, J.-Q. Huang, *Angew. Chem. Int. Ed.* **2023**, *62*, e202306889.
[29] M. Yeddala, L. Rynearson, B. L. Lucht, *ACS Energy Lett.* **2023**, *8*, 4782.
[30] N. Piao, S. Liu, B. Zhang, X. Ji, X. Fan, L. Wang, P.-F. Wang, T. Jin, S.-C. Liou, H. Yang, J. Jiang, K. Xu, M. A. Schroeder, X. He, C. Wang, *ACS Energy Lett.* **2021**, *6*, 1839.
[31] X. Zhang, X. Cheng, X. Chen, C. Yan, Q. Zhang, *Adv. Funct. Mater.* **2017**, *27*, 1605989.
[32] J.-G. Han, M.-Y. Jeong, K. Kim, C. Park, C. H. Sung, D. W. Bak, K. H. Kim, K.-M. Jeong, N.-S. Choi, *J. Power Sources* **2020**, *446*, 227366.
[33] X. Li, L. Guo, J. Li, E. Wang, T. Liu, G. Wang, K. Sun, C. Liu, Z. Peng, *ACS Appl. Mater. Interfaces* **2021**, *13*, 26023.
[34] J. Zhang, X. Yue, Z. Wu, Y. Chen, Y. Bai, K. Sun, Z. Wang, Z. Liang, *Nano Lett.* **2023**, *23*, 9609.
[35] J. Zheng, Y. Qiu, S. Liao, Z. Yue, S. Fang, N. Zhou, Y. Li, Y. Jiang, *Small* **2024**, *20*, 2405853.
[36] L. Qiao, S. Rodriguez Peña, M. Martínez-Ibañez, A. Santiago, I. Aldalur, E. Lobato, E. Sanchez-Diez, Y. Zhang, H. Manzano, H. Zhu, M. Forsyth, M. Armand, J. Carrasco, H. Zhang, *J. Am. Chem. Soc.* **2022**, *144*, 9806.
[37] Y. Meng, J. Li, S. Gu, Y. Fu, Z. Wang, J. Liu, X. Gong, *Electrochim. Acta* **2023**, *449*, 142262.
[38] W. Zhang, S. Zhang, L. Fan, L. Gao, X. Kong, S. Li, J. Li, X. Hong, Y. Lu, *ACS Energy Lett.* **2019**, *4*, 644.
[39] I. Hussain, S. Fatima, M. Tabish, *Spectrochim. Acta. A. Mol. Biomol. Spectrosc.* **2024**, *304*, 123408.
[40] K. Xu, *Chem. Rev.* **2004**, *104*, 4303.
[41] B. D. Adams, J. Zheng, X. Ren, W. Xu, J. Zhang, *Adv. Energy Mater.* **2018**, *8*, 1702097.
[42] G. Zheng, Y. Xiang, S. Chen, S. Ganapathy, T. W. Verhallen, M. Liu, G. Zhong, J. Zhu, X. Han, W. Wang, W. Zhao, M. Wagemaker, Y. Yang, *Energy Storage Mater.* **2020**, *29*, 377.
[43] C. Yan, X.-B. Cheng, C.-Z. Zhao, J.-Q. Huang, S.-T. Yang, Q. Zhang, *J. Power Sources* **2016**, *327*, 212.
[44] D. Wang, H. Liu, M. Li, D. Xia, J. Holoubek, Z. Deng, M. Yu, J. Tian, Z. Shan, S. P. Ong, P. Liu, Z. Chen, *Nano Energy* **2020**, *75*, 104889.
[45] S. H. Lee, J.-Y. Hwang, S.-J. Park, G.-T. Park, Y.-K. Sun, *Adv. Funct. Mater.* **2019**, *29*, 1902496.
[46] E. Peled, S. Menkin, *J. Electrochem. Soc.* **2017**, *164*, A1703.
[47] B. Liu, J.-G. Zhang, W. Xu, *Joule* **2018**, *2*, 833.
[48] X.-Q. Zhang, X.-B. Cheng, X. Chen, C. Yan, Q. Zhang, *Adv. Funct. Mater.* **2017**, *27*, 1605989.
[49] M. S. Kim, Z. Zhang, J. Wang, S. T. Oyakhire, S. C. Kim, Z. Yu, Y. Chen, D. T. Boyle, Y. Ye, Z. Huang, W. Zhang, R. Xu, P. Sayavong, S. F. Bent, J. Qin, Z. Bao, Y. Cui, *ACS Nano* **2023**, *17*, 3168.
[50] Y. Lei, X. Xu, J. Yin, K. Xi, L. Wei, J. Zheng, Y. Wang, H. Wu, S. Jiang, Y. Gao, *Small* **2024**, *20*, 2400365.
[51] J.-X. Chen, X.-Q. Zhang, B.-Q. Li, X.-M. Wang, P. Shi, W. Zhu, A. Chen, Z. Jin, R. Xiang, J.-Q. Huang, Q. Zhang, *J. Energy Chem.* **2020**, *47*, 128.
[52] B. Tong, Z. Song, H. Wan, W. Feng, M. Armand, J. Liu, H. Zhang, Z. Zhou, *InfoMat* **2021**, *3*, 1364.
[53] M. Ma, M. Du, Y. Liu, H. Lü, J. Yang, Z. Hao, J. Guo, X. Wu, *Particuology* **2024**, *86*, 160.
[54] X.-L. Wu, L.-Y. Jiang, F.-F. Cao, Y.-G. Guo, L.-J. Wan, *Adv. Mater.* **2009**, *21*, 2710.
[55] B. Jagger, M. Pasta, *Joule* **2023**, *7*, 2228.
[56] Y. Lei, X. Xu, J. Yin, J. Xu, K. Xi, L. Wei, H. Wu, S. Jiang, Y. Gao, *ACS Appl. Mater. Interfaces* **2023**, *15*, 46941.
[57] D. Lv, J. Zheng, Q. Li, X. Xie, S. Ferrara, Z. Nie, L. B. Mehdi, N. D. Browning, J.-G. Zhang, G. L. Graff, J. Liu, J. Xiao, *Adv. Energy Mater.* **2015**, *5*, 1402290.
[58] S. Jiao, J. Zheng, Q. Li, X. Li, M. H. Engelhard, R. Cao, J.-G. Zhang, W. Xu, *Joule* **2018**, *2*, 110.
[59] B. Yoon, J. Park, J. Lee, S. Kim, X. Ren, Y. M. Lee, H.-T. Kim, H. Lee, M.-H. Ryou, *ACS Appl. Mater. Interfaces* **2019**, *11*, 31777.

Manuscript received: March 25, 2025
Revised manuscript received: May 31, 2025
Version of record online: